Dalton Transactions

Dynamic Article Links

Cite this: *Dalton Trans.*, 2011, **40**, 2875

www.rsc.org/dalton

PAPER

Hexa- and octanuclear iron(III) salicylaldoxime clusters†

Kevin Mason,[a] Ian A. Gass,[a] Fraser J. White,[a] Giannis S. Papaefstathiou,[b] Euan K. Brechin*[a] and Peter A. Tasker*[a]

Received 16th November 2010, Accepted 17th January 2011
DOI: 10.1039/c0dt01593h

The syntheses, structures and magnetic properties of six iron complexes stabilised with the derivatised salicylaldoxime ligands Me-saoH$_2$ (2-hydroxyethanone oxime) and Et-saoH$_2$ (2-hydroxypropiophenone oxime) are discussed. The four hexanuclear and two octanuclear complexes of formulae $[Fe_8O_2(OMe)_4(Me\text{-}sao)_6Br_4(py)_4]\cdot 2Et_2O\cdot MeOH$ (**1**·2Et$_2$O·MeOH), $[Fe_8O_2(OMe)_{3.85}(N_3)_{4.15}(Me\text{-}sao)_6(py)_2]$ (**2**), $[Fe_6O_2(O_2CPh\text{-}4\text{-}NO_2)_4(Me\text{-}sao)_2(OMe)_4Cl_2(py)_2]$ (**3**), $[Fe_6O_2(O_2CPh\text{-}4\text{-}NO_2)_4(Et\text{-}sao)_2(OMe)_4Cl_2(py)_2]\cdot 2Et_2O\cdot MeOH$ (**4**·2Et$_2$O·MeOH), $[HNEt_3]_2[Fe_6O_2(Me\text{-}sao)_4(SO_4)_2(OMe)_4(MeOH)_2]$ (**5**) and $[HNEt_3]_2[Fe_6O_2(Et\text{-}sao)_4(SO_4)_2(OMe)_4(MeOH)_2]$ (**6**) all are built from a series of edge-sharing $[Fe_4(\mu_4\text{-}O)]^{10+}$ tetrahedra. Complexes **1** and **2** display a new μ_4-coordination mode of the oxime ligand and join a small group of Fe-phenolic oxime complexes with nuclearity greater than six.

Introduction

Polymetallic clusters of iron are being synthesised and studied for a host of reasons. In bioinorganic chemistry, for example, they have been employed as models for iron-containing enzymes such as methane monooxygenase and hemerythrin which both contain diiron cores, whilst the formation of larger oxy-hydroxy stabilised molecules can give insight into the formation and function of Ferritin, a protein containing up to ~4500 Fe centres that stores and regulates iron in living organisms.[1–3] The presence of five unpaired electrons in high spin Fe^{3+} ions also makes them attractive for making magnetically interesting complexes, and the triangular $[Fe_3O]^{7+}$ and tetrahedral $[Fe_4O]^{10+}$ building blocks common to the cores of many polymetallic Fe^{3+} cluster compounds can lead to fascinating frustration effects.[4] Geometric frustration is at the origin of a variety of phenomena such as spin glass behaviour or the appearance of unusual jumps and plateaus in the field-dependence of the magnetisation observed in antiferromagnetic $[Fe_3]$ triangles, $[Fe_{13}]$ Keggin ions and $[Fe_{30}]$ icosidodecahedra – properties reminiscent of those observed in extended frustrated lattices such as the Kagomé lattice.[5–7] An added effect of spin frustration is the presence of degenerate or low-lying excited spin states, a property that can be exploited in low-temperature magnetic refrigeration,[8] with clusters such as $[Fe_{14}]$ displaying an enhanced magnetocaloric effect.[9,10]

Salicylaldoxime ligands (Fig. 1) have been studied extensively for their use in extractive hydrometallurgy, showing great selectivity for Cu^{2+} and accounting for approximately 25% of the world's copper production.[11–13] Our research into Fe-salicylaldoximate complexes is fuelled not only by an interest in their magnetic properties, but also due to their role as anti-corrosives in protective coatings, where phenolic oximes have been used to treat lightly oxidised Fe surfaces.[14] It is postulated that the corrosion inhibition is due to the formation of polynuclear complexes on the surface and thus an extensive knowledge of the coordination chemistry of such ligands with Fe would tell us more about possible modes-of-action of the corrosion inhibition ability of the ligands. Herein we report the syntheses, structures and magnetic behaviour of four hexa- and two octametallic iron complexes built with the derivatised salicylaldoxime ligands Me-saoH$_2$ (2-hydroxyethanone oxime) and Et-saoH$_2$ (2-hydroxypropiophenone oxime).

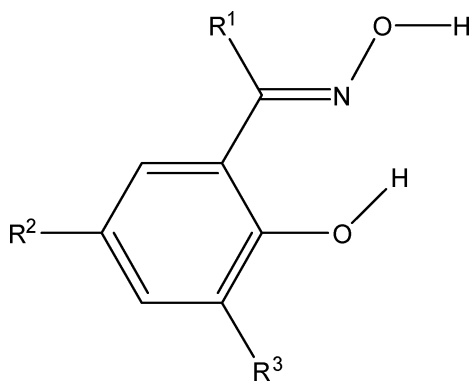

Fig. 1 General structure of the (derivatised) salicylaldoxime ligands. Me-saoH$_2$, R^1 = Me and R^2, R^3 = H; Et-saoH$_2$ R^1 = Et and R^2 and R^3 = H.

[a]*School of Chemistry, The University of Edinburgh, West Mains Road, Edinburgh, UK EH9 3JJ. E-mail: ebrechin@staffmail.ed.ac.uk, Peter.Tasker@ed.ac.uk; Tel: +44 (0) 131-650-7545*
[b]*Laboratory of Inorganic Chemistry, Department of Chemistry, National and Kapodistrian University of Athens, Panepistimiopolis, 157 71, Zografou, Greece*

† CCDC reference numbers 667681, 667684, 794871–794875. For crystallographic data in CIF or other electronic format see DOI: 10.1039/c0dt01593h

Experimental

Syntheses

All manipulations were performed under aerobic conditions using chemicals as received, unless otherwise stated. 2-Hydroxyethanone oxime (Me-saoH_2) and 2-hydroxypropiophenone oxime (Et-saoH_2) were synthesised *via* the reaction of the appropriate ketone with hydroxylamine and sodium acetate in EtOH, as described in the literature.[15] Complex **5** has been reported previously[16] but is included here to aid discussion.

$[Fe_8O_2(OMe)_4(Me\text{-}sao)_6Br_4(py)_4]\cdot 2Et_2O\cdot MeOH$ (**1**·2Et_2O·MeOH)

$FeBr_3$ (148 mg, 0.50 mmol) and Me-saoH_2 (226.5 mg, 1.50 mmol) were dissolved in MeOH (25 ml) in the presence of pyridine (2 ml). The dark red solution was stirred for 2 h, filtered and then diffused with Et_2O, producing X-ray quality crystals of **1** after 1 week, in approximately 20% yield. Elemental analysis found (calc.%) for $C_{81}H_{98}Br_4Fe_8N_{10}O_{21}$: C 41.73 (42.04), H 4.16 (4.27), N 5.97 (6.05).

$[Fe_8O_2(OMe)_{3.85}(N_3)_{4.15}(Me\text{-}sao)_6(py)_2]$ (**2**)

$FeF_3\cdot 3H_2O$ (167 mg, 1.00 mmol) and Me-saoH_2 (151 mg, 1.00 mmol) were dissolved in a mixture of MeOH (25 ml) and pyridine (2 ml) and stirred for 5 min. NaN_3 (130 mg, 2.00 mmol) was then added and the dark red solution was stirred for a further 120 min. The solution was filtered and left to evaporate slowly, producing X-ray quality crystals of **2** after 3 days in approximately 20% yield. Elemental analysis found (calc.%) for $C_{72}H_{73}Fe_8N_{23}O_{18}$: C 43.14 (43.34), H 3.42 (3.69), N 16.02 (16.15).

$[Fe_6O_2(OMe)_4(O_2CPh\text{-}4\text{-}NO_2)_4(Me\text{-}sao)_2Cl_2(py)_2]$ (**3**)

$FeCl_3\cdot 6H_2O$ (270 mg, 1.00 mmol), Me-saoH_2 (151 mg, 1.00 mmol) and $NaO_2CPh\text{-}4\text{-}NO_2$ (189 mg, 1.00 mmol) were dissolved in MeOH (25 ml) in the presence of pyridine (2 ml). The dark red solution was stirred for 2 h, filtered and then diffused with Et_2O, producing X-ray quality crystals of **3** after 1 week. The yield was approximately 30%. Elemental analysis found (calc.%) for $C_{61}H_{61}Cl_2Fe_6N_8O_{28}$: C 40.94 (41.26), H 3.05 (3.49), N 6.26 (6.37).

$[Fe_6O_2(OMe)_4(O_2CPh\text{-}4\text{-}NO_2)_4(Et\text{-}sao)_2Cl_2(py)_2]\cdot 2Et_2O\cdot MeOH$ (**4**·2Et_2O·MeOH)

The synthesis was identical to that of compound **3** using Et-saoH_2 (165 mg, 1.00 mmol) instead of Me-saoH_2. The yield was approximately 30%. Elemental analysis found (calc.%) for $C_{69}H_{80}Cl_2Fe_6N_8O_{29}$: C 43.45 (43.82), H 4.04 (4.26), N 5.77 (5.92).

$[HNEt_3]_2[Fe_6O_2(OMe)_4(Me\text{-}sao)_4(SO_4)_2(MeOH)_2]$ (**5**)

$Fe_2(SO_4)_3\cdot 6H_2O$ (508 mg, 1.00 mmol) and Me-saoH_2 (151 mg, 1.00 mmol) were dissolved in a solution of MeOH (30 ml) in the presence of NEt_3 (404 mg, 4 mmol). The solution was stirred for 1 h and then diffused with Et_2O, producing X-ray quality crystals after 3 days. The yield was approximately 30%. Elemental analysis found (calc.%) for $C_{50}H_{80}Fe_6N_6O_{24}S_2$: C 38.96 (38.78), H 5.10 (5.21), N 5.38 (5.43).

$[HNEt_3]_2[Fe_6O_2(OMe)_4(Et\text{-}sao)_4(SO_4)_2(MeOH)_2]$ (**6**)

The synthesis was identical to **5** using Et-saoH_2 (165 mg, 1.00 mmol) instead of Me-saoH_2. The yield was approximately 30%. Elemental analysis found (calc.%) for $C_{54}H_{88}Fe_6N_6O_{24}S_2$: C 40.38 (40.42), H 5.24 (5.53), N 5.20 (5.24).

Physical measurements

Elemental analyses (C, H, N) were performed by the EaStCHEM microanalysis service. Variable temperature magnetic susceptibility measurements were made on powdered polycrystalline samples restrained in eicosane using a Quantum Design MPMS-XL SQUID magnetometer equipped with a 7 T magnet. Diamagnetic corrections were applied using Pascal's constants.

Single crystal X-ray crystallography was performed using a Bruker Smart Apex CCD diffractometer equipped with an Oxford Cryosystems LT device, using Mo radiation. Data collection parameters and structure solution and refinement details are listed in Table 1. Full details can be found in the CIF files provided in the supporting information (CCDC 794871–7947875).†

Results and Discussion

Synthesis

Reacting $FeBr_3$ with Me-saoH_2 in a 1 : 3 ratio in a MeOH–pyridine solution yields the octanuclear complex $[Fe_8O_2(OMe)_4(Me\text{-}sao)_6Br_4(py)_4]$ (**1**), which has a metallic skeleton of two edge-sharing $[Fe_4O]$ tetrahedra, edge-capped by two additional Fe^{3+} ions. The oxime ligand displays a μ_4-coordination mode – the first time this has been observed. We can replace the terminal bromide ligands with terminal azides by simply introducing NaN_3 into the reaction mixture. This also has the effect of partially substituting a μ-methoxide bridge with an end-on μ-azide bridge affording the complex $[Fe_8O_2(OMe)_{3.85}(N_3)_{4.15}(Me\text{-}sao)_6(py)_2]$ (**2**). Further attempts to fully substitute the μ-methoxide bridges have proved unsuccessful, even when employing a large excess of NaN_3. Attempts to repeat these reactions with other iron halide salts have failed thus far. It is interesting to note that (in Fe^{3+} chemistry) only two examples of end-on bridging azides appear in the CCDC database – and both display ferromagnetic exchange coupling between the Fe^{3+} centres.[17,18]

Introducing carboxylates (in the form of $Na(O_2CPh\text{-}4\text{-}NO_2)$) to the reaction of $FeCl_3\cdot 6H_2O$ and Me-saoH_2 in a 1 : 1 : 1 ratio in a MeOH–py solution leads to the related but lower nuclearity hexanuclear complex $[Fe_6O_2(OMe)_4Cl_2(O_2CPh\text{-}4\text{-}NO_2)_4(Me\text{-}sao)_2(py)_2]$ (**3**). The core again consists of two edge-sharing tetrahedra but the replacement of the μ_4-bridging oximes with μ-bridging carboxylates prevents the addition of two additional edge-capping Fe^{3+} ions. Repeating the same reaction with Et-saoH_2 instead of Me-saoH_2 simply gives the analogous compound, $[Fe_6O_2(OMe)_4(O_2CPh\text{-}4\text{-}NO_2)_4(Et\text{-}sao)_2Cl_2(py)_2]$ (**4**). Despite many attempts, we failed to isolate compounds with carboxylates other than 4-NO_2-benzoate. It is unclear why this should be so, but we presume it to be due to the steric bulk of the 4-substituent and/or the stabilising inter-molecular interactions propagated between neighbouring NO_2 groups (*vide infra*).

The introduction of co-ligands, such as carboxylates, thus appears to favour the formation of smaller clusters and

Table 1 Crystallographic details for complexes **1–4**, **6**

	1·2Et$_2$O·MeOH	**2**	**3**	**4**·2Et$_2$O·MeOH	**6**
M/g mol^{-1}	2314.13	1985.63	1760.34	1891.41	1604.52
Crystal system	Hexagonal	Monoclinic	Triclinic	Monoclinic	Orthorhombic
Space group	$R\bar{3}$	$P2_1/c$	$P\bar{1}$	$P21/c$	*Pbca*
a/Å	42.1099(11)	11.9923(4)	16.1705(4)	13.5512(19)	20.4582(4)
b/Å	42.1099(11)	28.0040(10)	27.5304(7)	29.198(4)	14.4149(3)
c/Å	13.8971(4)	13.3217(5)	29.7123(8)	21.050(3)	22.6752(4)
α/°	90	90	114.5420(10)	90	90
β/°	90	114.382(2)	90.8730(10)	101.368(6)	90
γ/°	120	90	93.4590(10)	90	90
V/Å^3	21341.4(10)	4074.8(3)	11998.6(5)	8165(2)	6687.0(2)
T/K	150	150	100	100	150
Z	9	2	6	4	4
ρ_{calc}/g cm^{-3}	1.621	1.618	1.462	1.539	1.594
Crystal shape and colour	Black plate	Black plate	Black block	Black plate	Black block
Crystal size/mm	0.31 × 0.19 × 0.07	0.43 × 0.28 × 0.12	0.44 × 0.44 × 0.26	0.28 × 0.25 × 0.08	0.26 × 0.24 × 0.15
μ/mm^{-1}	2.943	1.463	1.205	1.187	1.410
Unique data	12 493	8336	48 626	15 647	5902
Unique data, ($I > 2\sigma(F)$)	7412	6650	31507	9754	5602
R_{int}	0.0560	0.0536	0.0531	0.0830	0.0689
*R*1[a], *wR*2[b]	0.0466, 0.1181	0.0424, 0.1012	0.0508, 0.1284	0.0701, 0.2073	0.0826, 0.1547
Goodness of fit	0.929	1.034	1.002	1.111	1.362

[a] *R*1) $\sum(|F_o| - |F_c|)/\sum|F_o|$ for observed reflections. [b] *wR*2) $\{\sum[w(F_o^2 - F_c^2)^2]/\sum[w(F_o^2)^2]\}^{1/2}$ for all data.

μ-coordination of the phenolic oxime. This is corroborated when sulfate anions are introduced to the reaction mixture. The reaction of $Fe_2(SO_4)_3{\cdot}6H_2O$ with Me-saoH$_2$ or Et-saoH$_2$ in the presence of NEt$_3$ in MeOH produces the hexanuclear complexes $[HNEt_3]_2[Fe_6O_2(Me\text{-}sao)_4(SO_4)_2(OMe)_4(MeOH)_2]$ (**5**) and $[HNEt_3]_2[Fe_6O_2(Et\text{-}sao)_4(SO_4)_2(OMe)_4(MeOH)_2]$ (**6**). The metallic core of both (analogous) molecules again comprises two edge-sharing [Fe$_4$O] tetrahedra but on this occasion each tripodal SO_4^{2-} anion caps one of the triangular faces of the tetrahedron, preventing further growth.

Description of structures

Complex **1** crystallises in the trigonal space group $R\bar{3}$ with nine molecules in the unit cell (Fig. 2). The metallic skeleton consists of two edge-sharing tetrahedra (Fe1–Fe2–Fe2′–Fe3 and symmetry equivalent, s.e.) with the Fe1 ⋯ Fe3 (and s.e) vertices capped by another Fe^{3+} ion (Fe4). The shared edge of the tetrahedra is defined by Fe2–Fe2′. Each [Fe^{III}_4] tetrahedron houses a central μ_4-O^{2-} ion (O123 and symmetry equivalent), with the bonding along the edges consisting of a combination of single O-atom bridges from μ-OMe^- ions and double N–O atom bridges from Me-sao^{2-} ligands. The latter display three different bonding modes: $\eta^2{:}\eta^1{:}\eta^2{:}\mu_4$, $\eta^1{:}\eta^1{:}\eta^2{:}\mu_3$ and $\eta^1{:}\eta^1{:}\eta^1{:}\mu$. The μ-Me-$sao^{2-}$ ligands bridge Fe2′–Fe3 (and s.e.) through the NO oximic group; the μ_3-Me-sao^{2-} ligands bridge Fe1–Fe4 and Fe3–Fe4 through the two atom N—O bridge and Fe1–Fe3 through the μ-oximic O-atom; and the μ_4-Me-sao^{2-} ligand – seen here for the first time – bridges Fe1, Fe4 and Fe4 through the NO double atom bridge and Fe1 and Fe2 through the phenolic O-atom. This tetranucleating motif for the salicylaldoxime may provide an explanation for how such ligands attach to lightly corroded iron surfaces when they are used as anti-corrosives.[14]

There are two symmetry inequivalent OMe^- ions: one bridges the edge-capping peripheral Fe^{3+} ion (Fe4) to the central tetrahedron (Fe3), and the other bridges across one edge of the central tetrahedron (Fe1–Fe2 and s.e). Each Fe^{3+} ion is in a distorted octahedral geometry (*cis*, 74.3(1)-107.1(1)°; *trans*, 156.4(1)-177.12(7)°) with FeO_5N (Fe2, Fe3), FeO_5Br (Fe1) and FeO_3N_2Br (Fe4) coordination spheres. The remaining coordination sites on Fe1, Fe3 and Fe4 are filled with a combination of terminally bonded Br^- ions and/or pyridine molecules.

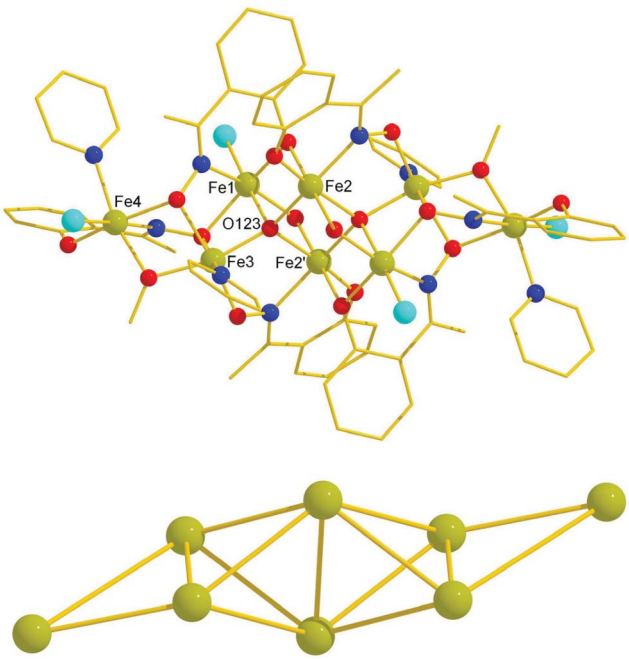

Fig. 2 The molecular structure of **1** (top) and its metallic core (bottom). Colour code: Fe = olive green; O = red; N = dark blue; C = gold; Br = light blue.

In the crystal, the molecules interact through two complementary C–H ⋯ π interactions [C5E–H5E ⋯ π (C1A, C2A, C3A,

C4A, C5A, C6A), C···centroid 3.543 Å, C–H···centroid 124°] to form one-dimensional (1D) chains running along the *c*-axis (Fig. 3). Despite the absence of any other inter-molecular hydrogen bonds or π···π interactions [the closest inter-molecular contacts being between the phenyl ring of the μ_4-Me-sao^{2-} ligand and a neighbouring pyridine molecule (C···C, 3.321(7) Å) and between methyl and phenyl groups on opposing μ_3-Me-sao^{2-} ligands (C···C, 3.362(5) Å)], when viewed down the *c*-axis the chains of **1** pack in groups of three around the three-fold screw axes (either left or right handed) imposed by the rhombohedral lattice to create large hexagonal cavities approximately 11 Å in diameter (Fig. 3).

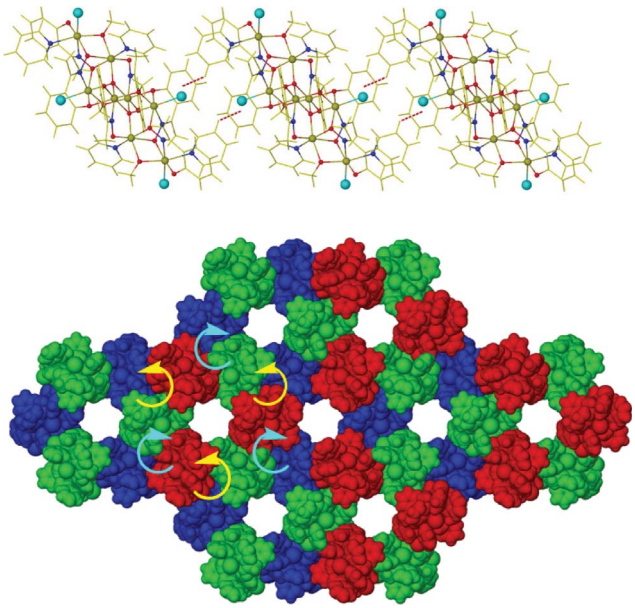

Fig. 3 The 1D chains of **1** along the *c*-axis formed through C–H···π interactions (top). Packing diagram of the chains of **1** (in red, blue and green) around the left handed (yellow arrow) and right handed (cyan) three-fold screw axes, emphasizing the hexagonal cavities (bottom).

Complex **2** crystallises in the monoclinic space group $P2_1/c$ with two molecules in the unit cell. The molecule differs only slightly from **1**. Besides the small changes in bond lengths and angles, the obvious differences are the replacement of the terminal bromide ions with terminally bonded azide ligands and the partial replacement of a μ-OMe$^-$ bridge with an end-on μ-N_3^- bridge (15% on Fe1–Fe2). This is an interesting observation since the introduction of end-on bridging azides to Fe^{3+} cluster chemistry is likely to produce molecules exhibiting ferromagnetic nearest neighbour exchange.[17,18] All Fe^{3+} ions have distorted octahedral geometries with *cis* angles in the range 74.09(9)–107.78(9)° and *trans* angles in the range 156.75(9)–179.4(1)°. There are no inter-molecular hydrogen bonds in the extended lattice with the closest contacts being between the phenyl ring of the μ_4-Me-sao^{2-} ligand and a neighbouring pyridine molecule (C···C 3.370(5) Å).

Complex **3** (Fig. 4) crystallises in the triclinic space group $P\bar{1}$ with three molecules in the asymmetric unit and two asymmetric units in the unit cell. The metallic core consists of two edge-sharing (Fe3–Fe4) tetrahedra (Fe1, Fe3, Fe4, Fe5 and Fe2, Fe3, Fe4, Fe6), each housing a central μ_4-O^{2-} ion (O134, O234). The two tetrahedral subunits are joined together by the two $\eta^1{:}\eta^1{:}\eta^2{:}\mu_3$-Me-sao^{2-} ligands bridging Fe1–Fe2 through their oximic NO moieties. The μ-oximic O-atom of one then bridges Fe1–Fe4 while the other bridges Fe2–Fe3. The four μ-O_2CPh-4-NO_2 and four μ-OMe$^-$ ligands bridge the remaining vertices, the carboxylates bridging Fe2–Fe3, Fe3–Fe5, Fe4–Fe5 and Fe4–Fe6 in their familiar *syn*, *syn*, μ-mode and the μ-OMe$^-$ bridging Fe1–Fe5, Fe2–Fe3, Fe3–Fe5 and Fe4–Fe6. The two remaining coordination sites on Fe5 and Fe6 are both occupied with one pyridine molecule and one halide ligand. Each Fe^{3+} ion is a distorted octahedral geometry (*cis*, 77.9(1)–103.9(1)°; *trans*, 157.6(1)–177.7(1)°) with FeO_6 (Fe3, Fe4), FeO_5N (Fe1, Fe2) and FeO_4NCl (Fe5, Fe6) coordination spheres. In the crystal there are a number of inter-molecular interactions propagated through neighbouring 4-NO_2 groups of the carboxylates (O···O, 3.011(4)–3.184(4) Å), as well as between the chloride ions and neighbouring pyridine molecules (Cl···C, 3.400(6) Å).

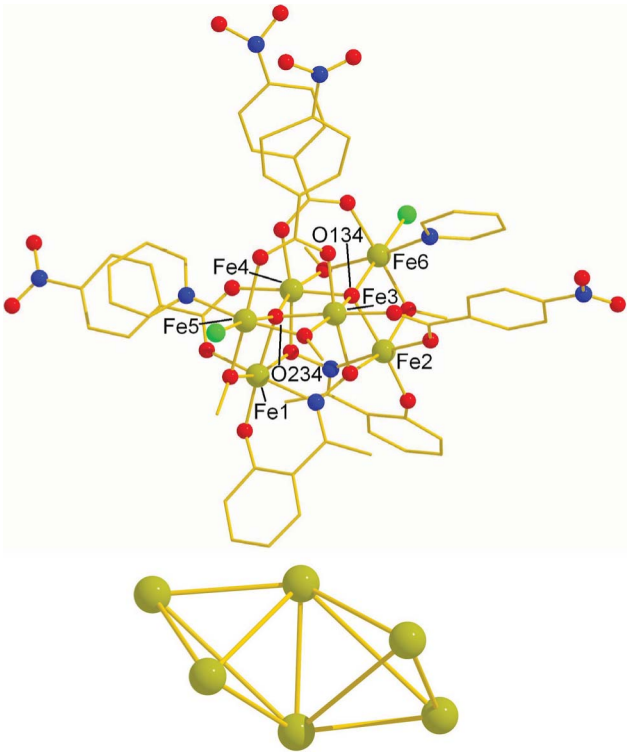

Fig. 4 The molecular structure of **3** (top) and its metallic core (bottom). Colour code: Fe = olive green; O = red; N = blue; C = gold; Cl = bright green.

Complex **4** crystallises in monoclinic $P2_1/c$ space group with four molecules in the unit cell. **4** differs from **3** only in the identity of the phenolic oxime, Et-sao^{2-} replacing Me-sao^{2-} and the intra-molecular bond lengths and angles are very similar in both compounds. In the crystal lattice there are inter-molecular hydrogen bonds between the 4-NO_2 group of carboxylate ligands and MeOH solvent molecules (O···C, 3.00(1) Å), with the shortest contact between neighbouring cluster molecules (3.40(1) Å) being between C-atoms on the phenyl rings of adjacent carboxylate and Me-sao^{2-} ligands.

Complex **6** (Fig. 5) crystallises in the orthorhombic space group *Pbca* with four molecules in the unit cell. Its structure is analogous to that of **5** (but containing Et-sao^{2-} rather than Me-sao^{2-}), which we have reported in a previous paper.[16] **6** is another

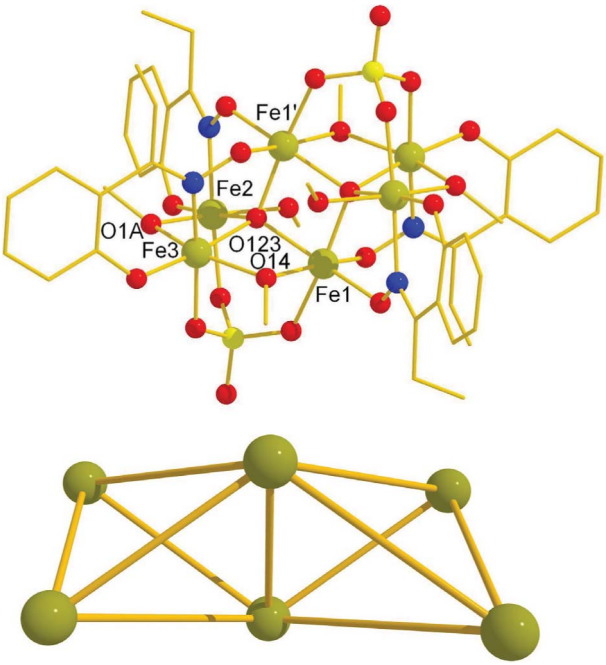

Fig. 5 The molecular structure of **6** (top) and its metallic core (bottom). Colour code: Fe = olive green; O = red; N = blue; C = gold; S = yellow.

example of an [Fe^{III}_6] cluster whose metallic core describes two edge sharing tetrahedra. The common edge is Fe1–Fe1′ with an inversion centre at its midpoint. The tetrahedra are built upon two central μ_4-O^{2-} ions (O123 and s.e.) and connected *via* four μ-OMe^- ions (O1A, O14 and s.e.) creating a $[Fe_6O_2(OMe)_4]^{10+}$ core similar to that observed in **3** and **4**. The $\eta^1{:}\eta^1{:}\eta^1{:}\mu_3$-$SO_4^{2-}$ ligands cap the Fe1–Fe2–Fe3 (and s.e.) triangular face of a tetrahedron, whilst the four $\eta^1{:}\eta^1{:}\eta^1{:}\mu$-Me-$sao^{2-}$ ligands bridge the Fe1–Fe2 and Fe1–Fe3 (and s.e.) edges. The remaining coordination sites on Fe1 and Fe1′ are filled by terminal MeOH molecules. The Fe^{3+} ions have FeO_6 (Fe1) or FeO_5N coordination spheres and lie in distorted octahedral geometries with *cis* angles in the range 76.9(2)–108.1(2)° and *trans* angles in the range 152.6(2)–175.4(2)°. An examination of the extended lattice reveals short contacts between the NEt_4^+ cation and the SO_4^{2-} (N···O, 2.82(1) Å), with the closest distances between neighbouring clusters being between the phenyl ring of the Et-sao^{2-} ligand and a SO_4^{2-} O-atom (C···O, 3.412(8) Å). There are also intra-molecular H-bonds present – between a terminally bonded MeOH molecule and an oximic O-atom (O···O, 2.737(6) Å). A scheme depicting the observed bridging modes of the R-sao^{2-} ligands is given in Fig. 6.

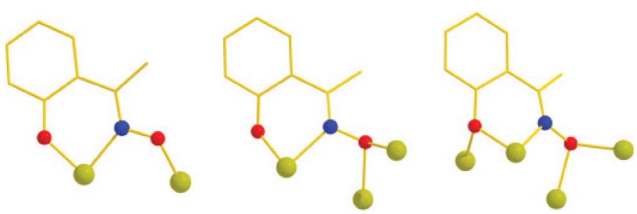

Fig. 6 The coordination modes of the phenolic oximes in complexes **1–6**. Colour code: Fe = olive green; O = red; N = blue; C = gold.

Discussion

There are now a number of Fe^{3+}/R-$saoH_2$ clusters in the literature (Table 2).[14,16,19–26] They range in size (≤ [Fe_{12}]) and structure, but there are undoubtedly some pervading themes. The body of published work in this area (Table 2) clearly shows that, akin to Mn^{3+}/R-$saoH_2$ chemistry, the $[Fe_3(\mu_3\text{-}O)]^{7+}$ triangle is the most frequently encountered building block.[26] The related tetrahedral subunit $[Fe_4(\mu_4\text{-}O)]^{10+}$ is the next most common, and this has no counterpart in Mn^{3+} chemistry. The variance in size of the [Fe_x] cluster can be attributed to a number of factors, including the presence or absence of co-ligand (here carboxylates and sulfates) and the steric bulk of the ketoxime group. This is another area in which we see a difference in comparison with the Mn^{3+} chemistry, where all of the above have little or no effect upon the products of the reaction.[27–29] The addition of (relatively large) bridging co-ligands tends to favour smaller nuclearity clusters (they edge- and face-cap preventing further growth) and encourages the μ-bridging mode of the phenolic oxime. In the absence of such co-ligands higher order bridging modes of R-sao^{2-} are seen (and higher nuclearity clusters as a consequence) and in complexes **1** and **2** the μ_4-bridging mode is seen for the very first time. The bridging modes depicted in Fig. 5 thus offer some insight into possible ligand bonding modes on lightly corroded iron surfaces when salicylaldoximes are used as anti-corrosives.[14]

Variations in the bulk of the ketoxime group can also change the topology of the cluster greatly in Fe^{3+} chemistry,[26] whereas in Mn^{3+} chemistry the $[M_3O(R\text{-}sao)_3]^+$ unit is almost always retained and the only differences observed appear to be in the twisting of the Mn–N–O–Mn torsion angles.[27] For example, both complex **1** and $[Fe_3O(OMe)(Ph\text{-}sao)_2Br_2(py)_3]\cdot Et_2O$[26] are made by reacting $FeBr_3$ with the appropriate R-$saoH_2$ pro-ligand in a MeOH–pyridine solvent mix. The bulky Ph-sao^{2-} ligand restricts the size of the cluster to an [Fe_3] triangle, but the Me-sao^{2-} ligand allows the growth of an octametallic cluster, [Fe_8].

When employing carboxylates in Fe^{3+}/R-$saoH_2$ chemistry one might expect the structures to resemble the basic Fe^{3+} carboxylates of general formula $[Fe_3O(O_2CR)_6L_3]^+$ (L = solvent) in which $\mu_{2/3}$-bridging R-sao^{2-} ligands simply replace the μ-bridging carboxylates. Indeed this is true in [Fe_6] clusters where the $[Fe_3(\mu_3\text{-}O)]^{7+}$ building block predominates,[23,24,26] and the μ_3-bridging oxime promotes oligomerisation of the basic triangles. Complexes **3** and **4** differ, the major change in reaction conditions being the introduction of pyridine. This results in the formation of a cluster adopting a metallic skeleton comprising two edge-sharing tetrahedra. Pyridine is present in excess and thus acts as base, ligand and co-solvent – a strategy that has been shown previously to aid the growth of very large mineral-like Fe^{3+} clusters.[30]

Magnetism

Direct current (dc) magnetic susceptibility measurements were performed on microcrystalline samples of representative **1** and **3** in a field of 0.1 T and in the 5–300 K temperature range. The magnetic behaviour of complex **5** is analogous to that of complex **6** which we have reported before, so will not be repeated here.[17] For **1** (Fig. 7) the room temperature $\chi_m T$ value of 12.38 cm^3 K mol^{-1} is significantly below the value of 35 cm^3 K mol^{-1} expected for eight non-interacting high spin ($S = 5/2$) Fe^{3+} ions, indicative

Table 2 The structurally characterised Fe/R-sao^{2-} complexes in the CCDC database

Molecule	Core	Oxime coordination	Ref.
$[HNEt_3][Fe_2(OMe)(Ph\text{-}sao)_2(Ph\text{-}saoH)_2]\cdot 5MeOH$	$[Fe_2(OMe)(NO)_2]^{3+}$ dimer	$2\times\mu$, $1\times$NO chelate	16
$[Fe_2(sao)_3(tmtacn)]\cdot MeOH$	$[Fe_2(NO)_3]^{3+}$ dimer	$3\times\mu$	21
$[Fe_2(3\text{-}5\text{-}di\text{-}^t but\text{-}sao)_3(tmtacn)]\cdot 3.5\ CHCl_3$	$[Fe_2(NO)_3]^{3+}$ dimer	$3\times\mu$	21
$[Fe_3O(O_2CPh)_5(sao)(MeOH)_2]\cdot 1.25MeOH\cdot 1.05H_2O$	$[Fe_3(\mu_3\text{-}O)]^{7+}$ triangle	$1\times\mu$	23
$[Fe_3O(O_2CPh)_5(sao)(EtOH)(H_2O)]\cdot EtOH$	$[Fe_3(\mu_3\text{-}O)]^{7+}$ triangle	$1\times\mu$	23
$[Fe_3O\ (O_2CPh)_5(Et\text{-}sao)(MeOH)_2]\cdot 3MeOH$	$[Fe_3(\mu_3\text{-}O)]^{7+}$ triangle	$1\times\mu$	16
$[Fe_3O(OMe)(Ph\text{-}sao)_2Cl_2(py)_3]\cdot 2MeOH$	$[Fe_3(\mu_3\text{-}O)]^{7+}$ triangle	$1\times\mu$	26
$[Fe_3O(OMe)(Ph\text{-}sao)_2Br_2(py)_3]\cdot Et_2O]$	$[Fe_3(\mu_3\text{-}O)]^{7+}$ triangle	$1\times\mu$	26
$[HNEt_3][Fe_3O(salmpH_3)(sao)_2(saoH)].2H_2O$	$[Fe_3(\mu_3\text{-}O)]^{7+}$ triangle	$1\times\mu$, $1\times$NO chelate	20
$[Fe_4(Me\text{-}sao)_4(Me\text{-}saoH)_4]\cdot MeOH$	Distorted $[Fe_4(NO)_4]^{8+}$ cube	$4\times\mu_3$, $4\times$NO chelate	16
$[Fe_4(Me\text{-}sao)_4(Me\text{-}saoH)_4]\cdot saoH_2\cdot C_8H_{10}$	Distorted $[Fe_4(NO)_4]^{8+}$ cube	$4\times\mu_3$, $4\times$NO chelate	14
$[Fe_4(Ph\text{-}sao)_4F_4(py)_4]\cdot 1.5MeOH$	$[Fe_4(NO)_4F_4]$ square	$4\times\mu$	26
$[Fe_4O_2(O_2CCH_3)_3(sao)_2(tmtacn)_2][PF_6]$	$[Fe_4(\mu_3\text{-}O)_2]^{8+}$ butterfly	$2\times\mu$	25
$[Fe_4O_2(O_2CC(OH)Ph_2)_3(sao)_2(tmtacn)_2][ClO_4]$	$[Fe_4(\mu_3\text{-}O)_2]^{8+}$ butterfly	$2\times\mu$	22
$[Fe_6O_2(O_2CPh)_{10}(sao)_2(MeCONH_2)2]\cdot 6MeCN$	$2\times[Fe_3(\mu_3\text{-}O)]^{7+}$ triangles	$2\times\mu_3$	24
$[Fe_6O_2(O_2CPh)_{10}(sao)_2(H_2O)_2]\cdot 2MeCN\cdot 3H_2O$	$2\times[Fe_3(\mu_3\text{-}O)]^{7+}$ triangles	$2\times\mu_3$	24
$[Fe_6O_2(OH)_2(O_2CPh)_6(Et\text{-}sao)_2(Et\text{-}saoH)_2]$	$2\times[Fe_3(\mu_3\text{-}O)]^{7+}$ triangles	$2\times\mu$, $2\times\mu_3$	26
$[HNEt_3]_2[Fe_6O_2(OH)_2(O_2CPh(Me)_2)_6(Et\text{-}sao)_4]\cdot 2MeCN$	$2\times[Fe_3(\mu_3\text{-}O)]^{7+}$ triangles	$2\times\mu$, $2\times\mu_3$	26
$[Fe_6Na_3O(OH)_4(OMe)_3(Me\text{-}sao)_6(H_2O)_3(MeOH)_6]\cdot MeOH$	$2\times[Fe_3(\mu_3\text{-}O)]^{7+}$ triangles	$6\times\mu$	26
$[Fe_6O_2(O_2CPh)_{10}(3\text{-}^t but\text{-}5\text{-}NO_2\text{-}sao)_2(H_2O)_2]\cdot 2MeCN$	$2\times[Fe_3(\mu_3\text{-}O)]^{7+}$ triangles	$2\times\mu$	26
$[Fe_6O_2(O_2CCH_2Ph)_{10}(3\text{-}^t but\text{-}sao)_2(H_2O)_2]\cdot 5MeCN$	$2\times[Fe_3(\mu_3\text{-}O)]^{7+}$ triangles	$2\times\mu$	26
$[HNEt_3]_2[Fe_6O_2(OMe)_4(Me\text{-}sao)_4(SO_4)_2(MeOH)_2]$	$2\times$edge sharing $[Fe_4(\mu_4\text{-}O)]^{10+}$ tetrahedra	$4\times\mu$	16/This paper
$[HNEt_3]_2[Fe_6O_2(OMe)_4(Et\text{-}sao)_4(SO_4)_2(MeOH)_2]$	$2\times$edge sharing $[Fe_4(\mu_4\text{-}O)]^{10+}$ tetrahedra	$4\times\mu$	This paper
$[Fe_6O_2(O_2CPhNO_2)_4(OMe)_4(Me\text{-}sao)_2Cl_2(py)_2]$	$2\times$edge sharing $[Fe_4(\mu_4\text{-}O)]^{10+}$ tetrahedra	$2\times\mu_3$	This paper
$[Fe_6O_2(OMe)_4(O_2CPhNO_2)_4(Et\text{-}sao)_2Cl_2(py)_2]$ $\cdot 2Et_2O\cdot MeOH$	$2\times$edge sharing $[Fe_4(\mu_4\text{-}O)]^{10+}$ tetrahedra	$2\times\mu_3$	This paper
$[Fe_8O_3(O_2CMe)_3(Me\text{-}sao)_3(tea)(teaH)_3]$	$3\times$common-edge sharing $[Fe_4(\mu_4\text{-}O)]^{10+}$ tetrahedra	$3\times\mu$	16
$[Fe_8O_3(O_2CMe)_3(Et\text{-}sao)_3(tea)(teaH)_3]$	$3\times$common-edge sharing $[Fe_4(\mu_4\text{-}O)]^{10+}$ tetrahedra	$3\times\mu$	16
$[Fe_8O_3(O_2CMe)_3(Ph\text{-}sao)_3(tea)(teaH)_3]$	$3\times$common-edge sharing $[Fe_4(\mu_4\text{-}O)]^{10+}$ tetrahedra	$3\times\mu$	16
$[Fe_8O_4(sao)_8(py)_4]\cdot 4py$	$4\times[Fe_4(\mu_4\text{-}O)]^{10+}$ tetrahedra	$4\times\mu$, $4\times\mu_3$	25
$[Fe_8O_2(OMe)_4(Me\text{-}sao)_6Br_4(py)_4]\cdot 2Et_2O\cdot MeOH$	$2\times$bicapped $[Fe_4(\mu_4\text{-}O)]^{10+}$ tetrahedra	$2\times\mu$, $2\times\mu_3$, $2\times\mu_4$	This paper
$[Fe_8O_2(OMe)_{3.85}(N_3)_{4.15}(Me\text{-}sao)_6(py)_2]$	$2\times$bicapped $[Fe_4(\mu_4\text{-}O)]^{10+}$ tetrahedra	$2\times\mu$, $2\times\mu_3$, $2\times\mu_4$	This paper
$[HNEt_3]_2[Fe_{12}Na_4O_2(OH)_8(OMe)_6(sao)_{12}(MeOH)_{10}]$	$4\times[Fe_3(\mu_3\text{-}O)]^{7+}$ triangles	$6\times\mu$, $6\times\mu_3$	26

Abbreviations: $saoH_2$, Ph-$saoH_2$, see Fig. 1. tmtacn, 1,4,7-trimethyl-1,4,7-triazacyclononane; $salmpH_3$, 2(bis(salicylideneamino)methyl)phenolate(−3); $teaH_3$, triethanolamine.

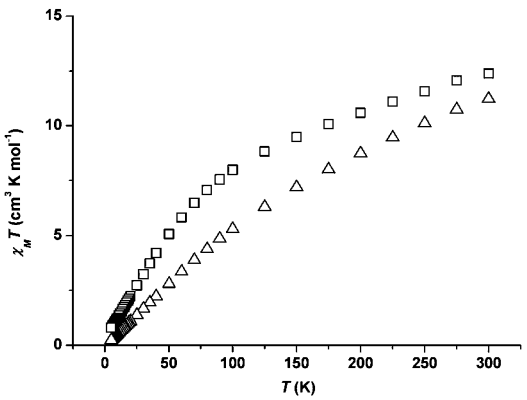

Fig. 7 Plot of $\chi_M T$ *vs.* T for complexes **1** (squares) and **3** (triangles).

of relatively strong antiferromagnetic exchange interactions. The $\chi_m T$ value decreases steadily with decreasing temperature reaching 0.79 cm^3 K mol^{-1} at 5 K, consistent with an $S = 0$ ground state. A plot of $1/\chi_m$ *vs.* T affords $\theta = -115$ K.

The room temperature $\chi_m T$ value of complex **3** is 11.23 cm^3 K mol^{-1}, lower than the expected value for six non-interacting Fe^{3+} ions (26.25 cm^3 K mol^{-1}). The $\chi_m T$ value then decreases constantly with decreasing temperature to a value of 0.25 cm^3 K mol^{-1}. This is again indicative of antiferromagnetic exchange interactions between the Fe^{3+} ions and the stabilisation of a diamagnetic ground state. A Curie–Weiss analysis of the $1/\chi_m$ *vs.* T plot affords $\theta = -386$ K. The complex nature of the structures precludes fitting of the susceptibility data by standard procedures. Of the thirty two complexes listed in Table 2 only two structural types (and a total of eight molecules) have been reported to possess non-zero spin ground states – the $[Fe_3]$ triangles and complexes **5** and **6**. Both are the result of spin frustration effects from antiferromagnetic exchange within symmetric metallic cores. This suggests that future attempts to build Fe^{3+}/R-sao^{2-} clusters with non-zero spin ground states should focus on the use of high temperature/high pressure (*e.g.* solvothermal or microwave) reaction conditions which are likely to produce highly symmetric molecules.[10]

Conclusions

The two hexa- and four octa-metallic Fe^{3+} salicylaldiminato clusters presented here all have a common building block, the tetrahedral $[Fe_4O]^{10+}$ moiety. Each contains a central core of two such edge-sharing tetrahedra, with **1** and **2** having two vertices additionally capped by Fe^{3+} ions, as a result of a unique μ_4-Me-sao^{2-} coordination mode. In contrast to Mn^{3+} complexes, the self-assembly of these Fe^{3+} molecules – and the coordination mode of the phenolic oxime ligand – appears to be highly dependent upon the presence of co-ligands and the steric bulk of the ketoxime group. The magnetic behaviour of all complexes is [perhaps unsurprisingly] dominated by relatively strong antiferromagnetic exchange interactions, as seen for almost all reported Fe^{3+}/R-saoH_2 complexes. However, the observation in complex **2** of the partial replacement of a μ-bridging OMe^- ion with an end-on μ-N_3^- ion, and the symmetric cores of complexes **5** and **6**, suggests targeting both azide-based clusters and highly symmetric complexes, since they may pave the way for isolating compounds displaying frustration effects, and/or ferro- or ferrimagnetic exchange interactions.

Notes and References

1 H. Basch, K. Mogi, D. G. Musaev and K. Morokuma, *J. Am. Chem. Soc.*, 1999, **121**, 7249.
2 E. C. Theil, *Annu. Rev. Biochem.*, 1987, **57**, 289; B. Xu and N. D. Chasteen, *J. Biol. Chem.*, 1991, **266**, 19965.
3 S. A. Malone, A. Lewin, M. A. Kilic, D. A. Svistuneko, C. E. Cooper, M. T. Wilson, N. E. Le Brun, S. Spiro and G. R. Moore, *J. Am. Chem. Soc.*, 2004, **126**, 496.
4 J. Schnack, *Dalton Trans.*, 2010, **39**, 4677.
5 J. Schnack, M. Luban and R. Modler, *Europhys. Lett.*, 2001, **56**, 863.
6 V. O. Garlea, S. E. Nagler, J. L. Zarestky, C. Stassis, D. Vaknin, P. Kögerler, D. F. McMorrow, C. Niedermayer, D. A. Tennant, B. Lake, Y. Qiu, M. Exler, J. Schnack and M. Luban, *Phys. Rev. B: Condens. Matter Mater. Phys.*, 2006, **73**, 024414.
7 J. van Slageren, P. Rosa, A. Caneschi, R. Sessoli, H. Casellas, Y. V. Rakitin, L. Cianchi, F. Del Giallo, G. Spina, A. Bino, A.-L. Barra, T. Guidi, S. Carretta and R. Caciuffo, *Phys. Rev. B: Condens. Matter Mater. Phys.*, 2006, **73**, 014422.
8 M. Evangelisti and E. K. Brechin, *Dalton Trans.*, 2010, **39**, 4672.
9 M. Evangelisti, A. Candini, A. Ghirri, M. Affronte, E. K. Brechin and E. J. L. McInnes, *Appl. Phys. Lett.*, 2005, **87**, 072504.
10 R. Shaw, R. H. Laye, L. F. Jones, D. M. Low, C. Talbot-Eeckelaers, Q. Wei, C. J. Milios, S. Teat, M. Helliwell, J. Raftery, M. Evangelisti, M. Affronte, D. Collison, E. K. Brechin and E. J. L. McInnes, *Inorg. Chem.*, 2007, **46**, 4968.
11 P. A. Tasker, P. G. Plieger and L. C. West, *Comprehensive Coordination Chemistry II*, 2004, **9**, 759.
12 G. A. Kordosky, *Proceedings of the International Solvent Extraction Conference*, Cape Town, South Africa, March 17–21, 2002, p. 853.
13 P. J. Mackey, *CIM Mag.*, 2007, **2**, 35.
14 J. M. Thorpe, R. L. Beddoes, D. Collison, C. D. Garner, M. Helliwell, J. M. Holmes and P. A. Tasker, *Angew. Chem., Int. Ed.*, 1999, **38**, 1119.
15 R. Dunsten and T. A. Henry, *J. Chem. Soc. Trans.*, 1899, **75**, 66.
16 I. A. Gass, C. J. Milios, A. Collins, F. J. White, L. Budd, S. Parsons, M. Murrie, S. P. Perlepes and E. K. Brechin, *Dalton Trans.*, 2008, 2043.
17 K. Rajender Reddy, M. V. Rajasekharan and J. –P. Tuchagues, *Inorg. Chem.*, 1998, **37**, 5978.
18 G. De Munno, T. Poerio, G. Viau, M. Julve and F. Lloret, *Angew. Chem., Int. Ed. Engl.*, 1997, **36**, 1459.
19 P. Chaudhuri, M. Winter, P. Fleischhauer, W. Haase, U. Florke and H.-J. Haupt, *Inorg. Chim. Acta*, 1993, **212**, 241.
20 E. Bill, C. Krebs, M. Winter, M. Gerdan, A. X. Trautwein, U. Florke, H.-J. Haupt and P. Chaudhuri, *Chem.–Eur. J.*, 1997, **3**, 193.
21 C. N. Verani, E. Bothe, D. Burdinski, T. Weyhermuller, U. Florke and P. Chaudhuri, *Eur. J. Inorg. Chem.*, 2001, 2161.
22 P. Chaudhuri, E. Rentschler, F. Birkelbach, C. Krebs, E. Bill, T. Weyhermuller and U. Florke, *Eur. J. Inorg. Chem.*, 2003, 541.
23 C. P. Raptopoulou, Y. Sanakis, A. K. Boudalis and V. Psycharis, *Polyhedron*, 2005, **24**, 711.
24 C. P. Raptopoulou, A. K. Boudalis, Y. Sanakis, V. Psycharis, J. M. Clemente-Juan, M. Fardis, G. Diamantopoulos and G. Papavassiliou, *Inorg. Chem.*, 2006, **45**, 2317.
25 I. A. Gass, C. J. Milios, A. G. Whittaker, F. P. A. Fabiani, S. Parsons, M. Murrie, S. P. Perlepes and E. K. Brechin, *Inorg. Chem.*, 2006, **45**, 5281.
26 K. Mason, I. A. Gass, S. Parsons, A. Collins, F. White, A. M. Z. Slawin, E. K. Brechin and P. A. Tasker, *Dalton Trans.*, 2010, **39**, 2727.
27 R. Inglis, L. F. Jones, C. J. Milios, S. Datta, A. Collins, S. Parsons, W. Wernsdorfer, S. Hill, S. P. Perlepes, S. Piligkos and E. K. Brechin, *Dalton Trans.*, 2009, 3403.
28 R. Inglis, L. F. Jones, K. Mason, A. Collins, S. A. Moggach, S. Parsons, S. P. Perlepes, W. Wernsdorfer and E. K. Brechin, *Chem.–Eur. J.*, 2008, **14**, 9117.
29 L. F. Jones, R. Inglis, M. E. Cochrane, K. Mason, A. Collins, S. Parsons, S. P. Perlepes and E. K. Brechin, *Dalton Trans.*, 2008, 6205.
30 G. W. Powell, H. N. Lancashire, E. K. Brechin, D. Collison, S. L. Heath, T. Mallah and W. Wernsdorfer, *Angew. Chem., Int. Ed.*, 2004, **43**, 5772.